Effects of Solidification Thermal Parameters and Bi Doping on Silicon Size, Morphology and Mechanical Properties of Al-15wt.% Si-3.2wt.% Bi and Al-18wt.% Si-3.2wt.% Bi alloys

Marcelino Dias [a], Ricardo Oliveira [a], Rafael Kakitani [a], Noé Cheung [a], Hani Henein [b], José Eduardo Spinelli [c], Amauri Garcia [a,*]

[a] *Department of Manufacturing and Materials Engineering, University of Campinas UNICAMP, 13083-860 - Campinas, SP, Brazil.*
[b] *Department of Chemical and Materials Engineering, University of Alberta, Edmonton, AB T6G 2G6 Canada.*
[c] *Department of Materials Engineering, Federal University of São Carlos, São Carlos, SP 13565-905 Brazil.*

Abstract

The use of bismuth (Bi) in aluminum (Al) industries is recognized as prime importance because of possible recycling as alloying element in special applications such as those enhancing machinability. The effects of Bi interaction on solidification progress as well as on the resulting microstructure of hypereutectic Al-Si alloys, i.e. the morphology and size of Si crystals are rare information. As such, the present research work investigates the characteristic parameters of eutectic and primary Si with addition of Bi for both ternary Al-15 wt.%Si- 3.2 wt.%Bi and Al-18 wt.%Si- 3.2 wt.%Bi alloys samples directionally solidified (DS) under various cooling rates. The alloy containing 15 wt.%Si showed that Bi acts in the suppression of the growth of primary Si crystals for samples solidified at cooling rates ranging from 2.0 to 31 K/s. For lower rates, a minor fraction of five-fold branched Si was recognized in transverse specimens. A mixture of globular-fibrous eutectic Si is shown to occur for eutectic cooling rates higher than 5 K/s. The Al-18 wt.%Si- 3.2 wt.%Bi alloy is characterized by a mixed structure of eutectic flaky Si and primary angular Si with intersecting spines at nearly 90º all over the entire range of experimental cooling rates (i.e., from 0.4 to 40 K/s). Despite the intricacy of the formed microstructures, it was possible to establish relationships between tensile properties and eutectic Si spacing in order to compare the properties between the tested alloys. Tensile strength and elongation decrease with increasing alloy Si content.

Keywords: Al-Si-Bi alloys; solidification; microstructure; tensile properties.

* Corresponding author → E-mail address: amaurig@fem.unicamp.br

1. Introduction

Al-Si alloys are widely used in the automotive industry. This is thanks to their high strength to weight ratio, suitable fluidity, good corrosion resistance and high productivity [1,2]. Hypereutectic Al-Si alloys are also considered important materials in the transportation sector as well as for high temperature applications [3,4].

Crystals of the α-Al solid solution and those of the pure Si are the main phases constituents of the Al-Si alloy microstructure. Considering thermodynamic equilibrium conditions and hypereutectic compositions, the following sequence is valid. At the first stage of solidification, the solid is formed by Si particles and at the next stage, these phases constitute the binary (αAl+Si) eutectic. According to Warmuzek [5] the equilibrium shape of primary Si is a regular octahedron, which is limited by facets equivalent to crystallographic planes {111}. However, different morphologies were already demonstrated to occur, such as spheres of rough surface, dendrites, deformed polyhedrons, plates, stars, or feathers. The many exceptions are due to the applied solidification cooling rate, alloy composition, undercooling of liquid alloy or overheating [6-8]. The eutectic Si, in its turn, may assume a shape of either flaky (lamella) or fiber (rod). The lamellae are mostly placed in between α-Al bands side by side, while the quickly growing fibers are embedded into a continuous matrix. Si in the shape of rods is demonstrated to be formed at high cooling rates [9,10]. The shape of globules of Si is also reported for fast cooling conditions, for instance, those attained during atomization. Very recently the prevalence of a globular Si eutectic morphology in impulse atomized Al-18 wt.%Si alloy powders was demonstrated for cooling rates higher than 55 K/s [11]. The solidification cooling rate was also shown to be decisive for the eutectic morphology, as reported by Reyes et al. [12]. In this research, Al-15 wt.%Si alloy samples were generated by transient directional solidification. It was demonstrated, for instance, that for rates exceeding 9 K/s a mixture of fibers and globules prevailed during the formation of Si.

Bearing in mind that the macroscopic materials properties such as mechanical strength and ductility are influenced by either shape or size of both primary and eutectic Si phases, occurrences of crystallization course such as spacing selection and morphological transitions must be evaluated as a result of solidification conditions. For the purpose of improving mechanical properties of Al-Si alloys, the practice of adding elements to control the microstructure has been largely employed. The effects of eutectic and primary silicon modifiers such as Na, Ca,

Sr, Sb, and P on microstructure of the Al-Si alloys are relatively well understood [13]. The main goal, in these cases, is enhancing mechanical properties of these alloys.

It is stated that the amount of Bi has increased in Al industries. This is explained by the interest in use of this element envisaging particular needs such as in enhancing machinability [14], promoting chip breaking during machining operations [15], optimizing tool lubrication [16] and disrupting the formation of oxide defects [17]. Al-Si alloys with quite substantial Bi content have been demonstrated to ensure enough self-lubricating performance for use in wearing components even under unwell lubricated conditions. The improved A356 alloy modified with Bi still demonstrated suitable strength and ductility [18]. Moreover, Bi is considered an alternate for lead (Pb) and phosphorous-sulfur (P-S) due to its non-toxicity [19].

It is also remarkable that Al industries have been progressing towards using secondary Al, which is a form to reduce the initial energy output of the Al productive chain. However, the use of secondary Al causes some drawbacks mostly associated with elemental contamination, which may affect, for instance, the melt treatment, i.e., operations such as grain refinement and eutectic modification. Due to that, understanding the effects of these additions has drawn researchers' attention. In view of the facts already mentioned regarding the use of Bi as additive as well as its presence in secondary Al, the microstructure-related aspects are an important technological step requiring further consideration.

Despite the increasing interest in Bi and their effects, only few research investigations are devoted to its resulting impacts on microstructure and mechanical properties of Al-Si alloys. For instance, the presence of Bi in hypoeutectic Al-Si alloys was demonstrated to produce refined eutectic Si crystals [20-22]. Farahany *et al.* [21] investigated the effect of Bi addition and the mechanism responsible for transforming the Si. It was shown that the refining effect is more related to the growth stage than to the nucleation step. Bi was observed to enrich the Al/Si interface and, as consequence, reducing the surface tension of Al in contact with the Si crystal. The improved local wetting tends to encapsulate the growing Si particles, inhibiting its growth. According to Durgrapasadu [23] the addition of 1.5 wt% of Bi in the hypereutectic Al-17.6 wt.% Si alloy promoted blunt corner Si particles to form; in contrast with sharp corner particles observed in the non-modified alloy. It is also reported that the hardness of the Bi-containing alloys was higher than that of the non-modified Al-Si alloy. Oppositely, inferior mechanical strength of a Bi-containing Al-Si alloy was reported by Okayasu *et al.* [24]. In this case, from tensile tests with the Al-$Si_{10.6}$-$Cu_{2.5}$ and (Al-$Si_{10.6}$-$Cu_{2.5}$)-$Bi_{0.5\text{-}1.5}$ alloys, it was shown that the

tensile strength decreased with increasing Bi additions. However, ductility was improved due to the same additions.

To the best of our knowledge, there are no studies available correlating the microstructure sizes and morphologies of Bi-containing hypereutectic Al-Si alloys parts by varying solidification parameters, such as cooling rate and growth velocity. A methodical investigation of microstructure evolution of hypereutectic Al-Si-Bi alloys produced at various cooling rates will offer an assessable knowledge on the size, morphology and strength related to the employed solidification conditions. For instance, the capability of conventional growth relationships regarding the eutectic solidification in this type of alloys persists unassessed up to now. One type of relationship to be faced is the traditional formula used for eutectics: $\lambda^2 v = C$ [25], where λ is the eutectic Si spacing; v is the solidification velocity and C a constant value.

In the present study, Al-15 and 18 wt.% Si hypereutectic alloys are modified with 3.2 wt.% Bi. The idea is to compare the effect of bismuth addition on the morphology of the phases forming the microstructure and on tensile properties. For that, previously available data for the binary Al-15 and Al-18Si alloys will be compared to those generated for both ternary alloys. Various samples characterized by distinct cooling rates were generated by transient directional solidification of the ternary Al-Si-Bi alloys. Firstly, the experimental evolutions of the cooling rate within the DS castings as well as the variations of the Si eutectic spacing will be compared to each other based on their trends. Secondly, the morphologies of both eutectic and primary Si crystals will be mapped as a function of parameters enlightening the processing history, i.e. cooling rate and growth rate. Finally, the effects of Bi addition on the tensile properties will be outlined.

2. Experimental procedure

Both ternary Al-15 wt.%Si- 3.2 wt.%Bi and Al-18 wt.%Si- 3.2 wt.%Bi alloys castings were generated using commercially pure Al (99.8 wt.%), Si (99.7 wt.%) and Bi (99.9 wt.%). Such elements were melted by using a SiC crucible inside a muffle furnace. Firstly, only Al was melted in a muffle furnace. After that, Silicon was added into the melt in small pieces and homogenized in order to be incorporated into the molten Al. The alloy was held for more 3 hours at a temperature of around 900 °C in the muffle furnace. Every one hour the alloy was removed from the furnace, homogenized and replaced into the furnace. Afterwards, bismuth was added to the

molten bath. Previous alloy standards were prepared to have their compositions determined, so that the optimized Bi content to be added could be established. Finally, the best procedure was chosen on extrapolating the Bi content in 50% higher than the nominal Bi alloying. This was necessary because Bi oxidizes without atmosphere control during melting, which was the case. The adopted time x temperature cycle was enough to guarantee that all the Si dissolved in the alloy avoiding the microstructure to show any particle of raw Si.

In the directional solidification system, shown in Fig. 1, the mold was built with a 3mm-thick steel bottom part (closure mold device). In the case of the present experiments, the active surface of the bottom part was ground by a #1200 grinding wheel. Consequently, a broad range of cooling rates during the solidification progress across the directionally solidified (DS) casting is achievable. Fine grinding the active surface of the bottom part could permit high cooling rates to be attained in the very first portions of the casting with respect to the cooled surface. The molten ternary Al-Si-Bi alloy was then poured into the directional solidification apparatus, and after natural solidification within the mold, the alloy was remelted *in situ* by radial electrical wiring positioned around a stainless-steel split mold, as can be seen in the scheme of Fig. 1. Then, when the melt temperature was about 10 % above the *liquidus* temperature, the electric heaters were disconnected and at the same time the water flow at the bottom of the container was started, which allowed the onset of directional solidification. The evolution of temperatures along the length of the casting was monitored by fine type K thermocouples (0.2 mm diameter wire), placed in the geometrical center of the cylindrical mold cavity, but in various relative positions along its length. The determination of solidification rates of cooling down was based in the passage of two isotherms along the length of the DS casting, which are *liquidus* and eutectic isotherms. The *liquidus* cooling rate, $\dot{T}_L$, as a function of position (P) in the casting was carried out by computing the time-derivative of each cooling curve (dT/dt) right after the passage of the *liquidus* isotherm by each thermocouple. The same procedure permitted determining the eutectic cooling rate, $\dot{T}_E$, while considering the displacement of the eutectic front as a reference for the calculations.

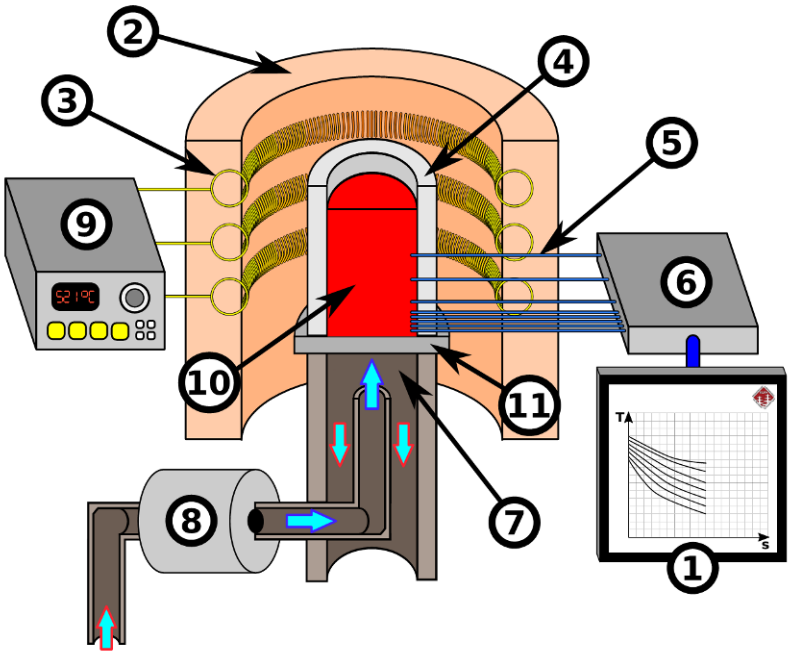

Fig. 1. Scheme of the upward directional solidification system used to generate the Al-Si-Bi alloy castings: 1 - acquired thermal profiles during experiment; 2 - ceramic support; 3 - electric resistances; 4 - stainless-steel split mold; 5 - thermocouples; 6 - data logger; 7 - water flow inlet; 8 - flowmeter; 9 - temperature controller; 10 - molten alloy and 11 - cooled bottom part.

The dimensions of the stainless-steel mold were: internal diameter of 60 mm, height of 157 mm and wall thickness of 5 mm. The lateral inner mold surface was covered with a 2 mm-thick layer of insulating mass of silica-alumina ceramic to minimize radial heat losses and assist the removal of the castings. Additional information on specific details of the directional solidification procedure can be found in previous studies [26,27].

The chemical composition of the Al-15%Si-3.2%Bi alloy casting was determined by optical emission spectroscopy (OES), giving as result a chemistry of 14wt%Si, 3.21wt%Bi and Al in balance. For the Al-18%Si-3.2%Bi alloy casting the analysis was carried out by X-ray fluorescence (XRF), resulting in 17.7wt.%Si, 3.22wt%Bi and Al in balance.

The considerations about microstructure were focused on two features, which were the spacing between the primary silicon, λ_{Sip}, and the eutectic Si spacing, λ_{Si}. Both microstructural spacings were assessed by using an optical microscope considering various slices removed from the DS castings. The methods used to determine such dimensions can be seen in Fig. 2. The mentioned parameters were considered the more appropriate ones in order to represent the effects of solidification conditions on the as-solidified microstructures. For this purpose, various

selected transverse (perpendicular to the growth direction) samples were extracted at different positions along the length of the DS casting for metallography.

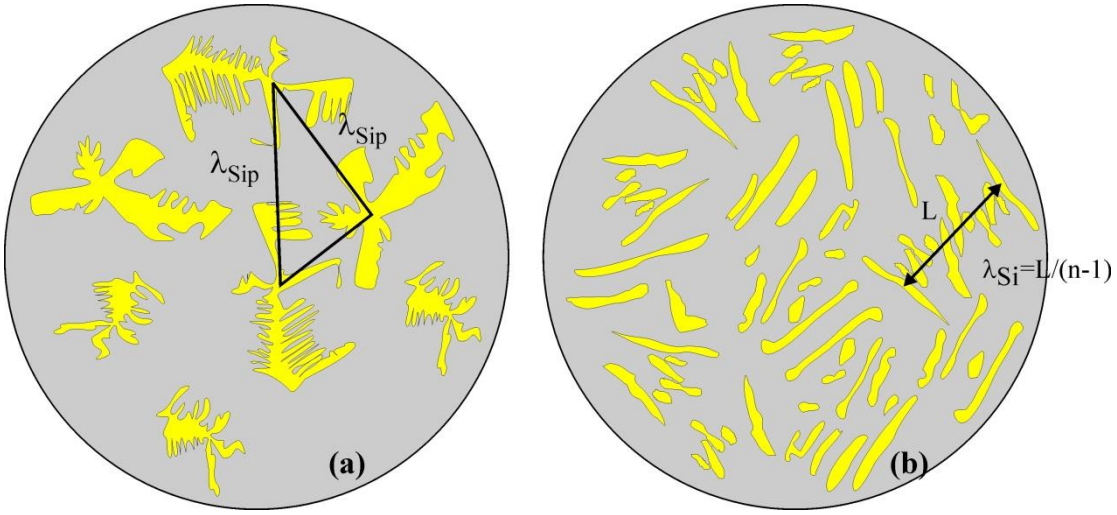

Fig. 2. Schematic representation of employed methods to measure (a) the primary silicon, λ_{Sip}, and (b) the eutectic Si spacing, λ_{Si}: triangle method for λ_{Sip} and intercept method for λ_{Si}.

The primary silicon, λ_{Sip}, and eutectic Si spacing, λ_{Si}, were measured from the optical images of the samples: about 30 measurements at each selected section. In order to reveal the formed phases and their morphologies, Scanning Electron Microscopy (SEM) analyzes were carried out on some of the samples. The instrument used was a Zeiss SEM (Zeiss-EVO-MA15) equipped with an Oxford-X-Max dispersive X-ray spectroscopy (EDS).

Transverse specimens were extracted from different positions along the length of the DS castings and prepared for tensile testing according to specifications of ASTM Standard E 8M. A strain rate of about 3×10^{-3} s^{-1} was adopted. In order to ensure the reproducibility of results, three specimens were tested for each selected position, and tensile properties were determined: ultimate tensile strength (σ_u) and elongation (δ).

3. Results and discussions

The experimental solidification cooling rates and growth rates for the Al-15 wt.%Si- 3.2 wt.%Bi and Al-18 wt.%Si- 3.2 wt.%Bi alloys were obtained from the experimental plots given in Fig. 3. Primary Si and eutectic

(α-Al+Si) mixture are the phases of interest since they are related to the formation of the Si crystals during alloy solidification. As such, two isotherms must be followed during the course of the directional solidification, that is, *liquidus* and eutectic. The *liquidus* and eutectic temperatures are indicated inside the graphs of Fig. 3. Calculations of the *liquidus* and eutectic cooling rates, $\dot{T}_L$, $\dot{T}_E$, as a function of position (P) in the casting were carried out by computing the time-derivative of each cooling curve (dT/dt) right after the passage of each of the mentioned isotherms through each thermocouple.

The cooling curves in Fig. 3 also enable combinations of pairs of position (P), from the cooled surface of the casting, and related times of the eutectic (t_E) and *liquidus* (t_L) isotherm tracks in each thermocouple. As such, pairs t_E x P and t_L x P are conceived. Experimental functions type P=f(t) fit the experimental scatters. A time-derivative of these functions resulted in the eutectic and *liquidus* growth rates (V_E, V_L).

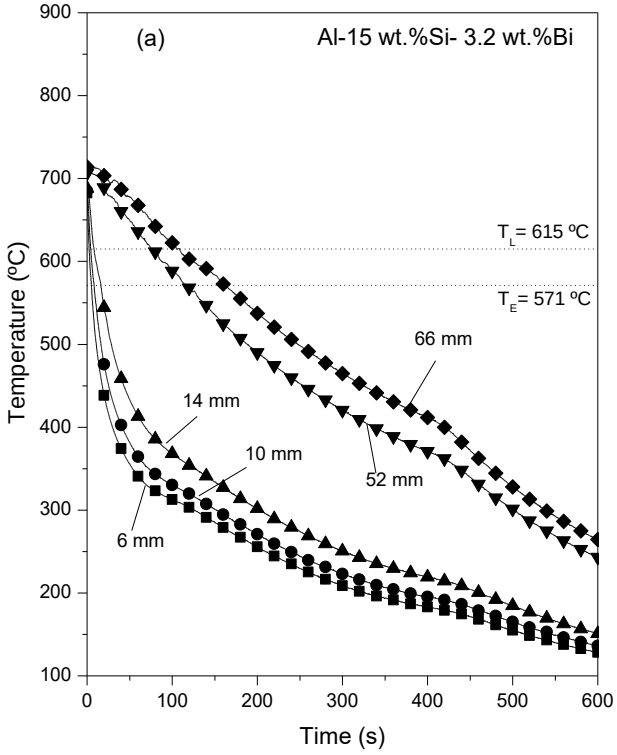

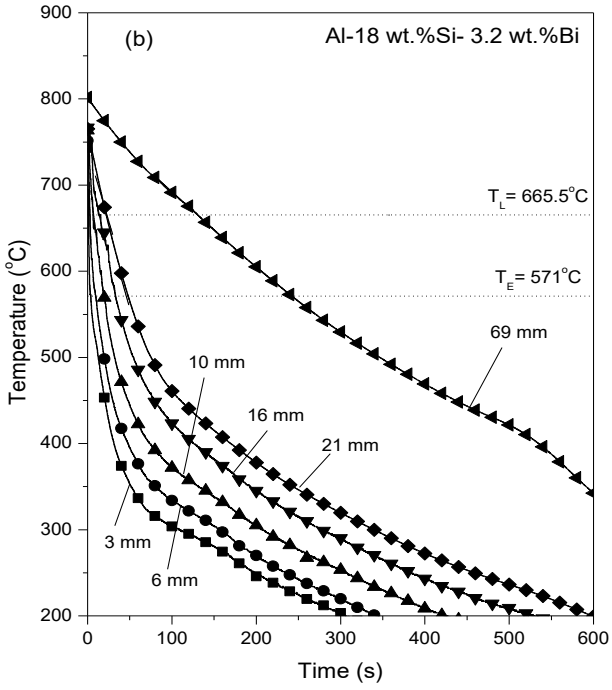

Fig. 3. Cooling curves at different positions within the DS (a) Al-15 wt.%Si-3.2 wt.%Bi and (b) Al-18 wt.%Si-3.2 wt.%Bi alloys castings. The signs within the graphs signify the positions in mm from the cooled surface of the casting.

A pseudo-binary phase diagram of the Al-Si-Bi system is shown in Fig. 4. The Thermo-Calc software provided the data to generate this diagram considering a fixed concentration of 3.2 wt.% Bi. This kind of calculation is very useful not only to provide the temperature transformations, but also to permit one to follow the solidification path of the alloys of interest, i.e., the Al-15 wt.%Si-3.2 wt.%Bi and Al-18 wt.%Si-3.2 wt.%Bi alloys. Besides indication of the first formed primary Si (Diamond_A4) followed by the eutectic reaction at 571.5 ºC, a very large 'Liquid' window from 571.5 ºC to 272 ºC can be seen. For temperatures below 272ºC this 'Liquid' converts into solid Bi (Rhombo_A7).

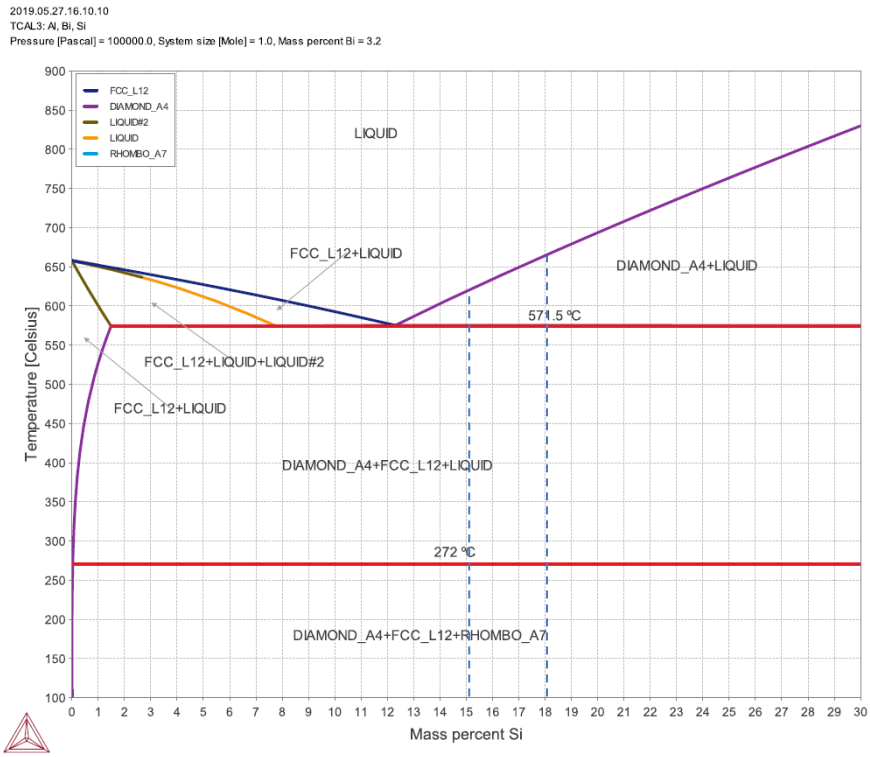

Fig. 4. Pseudo-binary Al-3.2 wt%Bi – (X)Si phase diagram computed using TCAL3 database of the Thermo-Calc software with signs of the studied chemistries.

Changes in cooling rates and growth rates across the DS castings are depicted in Fig. 5 and Fig. 6. Overall, it is worth noting that eutectic parameters related to the alloy containing 15 wt.% Si are larger than those related to the other composition. The same applies to the *liquidus* thermal parameters determined here. This means that Si content plays a decisive role on the heat transfer efficiency during solidification of the Al-Si-Bi alloys. For example, the cooling rate related to the eutectic front, $\dot{T}_E$, shifts at first solidification stages (i.e., P=5 mm in Fig. 5) from 18.8 to 8.4 K/s with varying alloy Si from 15 to 18 wt.%. Heat transfer efficiency mainly depends on wettability (i.e., fluidity), solidification freezing interval and thermosphysical properties [28,29]. At the beginning of solidification, heat transfer is controlled by the interfacial metal/mold heat transfer coefficient (h_i) of each alloy, that is, the higher h_i the higher the solidification cooling rate. The alloy fluidity is directly proportional to h_i, and according to a previous study, the fluidity of Al-Si alloys has its maximum value for a composition of about 18wt.%Si [30]. This has induced higher values of cooling rate at positions in the DS casting closer to the cooled mold, for the Al-18 wt.%Si -3.2 wt.%Bi alloy casting as compared to the Al-15 wt.%Si -3.2 wt.%Bi alloy casting, With the progress of solidification, the thermal resistance of the solidifying layer becomes much higher than that associated with h_i after a certain position in the DS casting, and the evolution of

solidification is then controlled by the alloy thermal properties, and consequently higher values of cooling rates are related to the Al-15 wt.%Si -3.2 wt.%Bi alloy casting, as shown in Fig. 5.

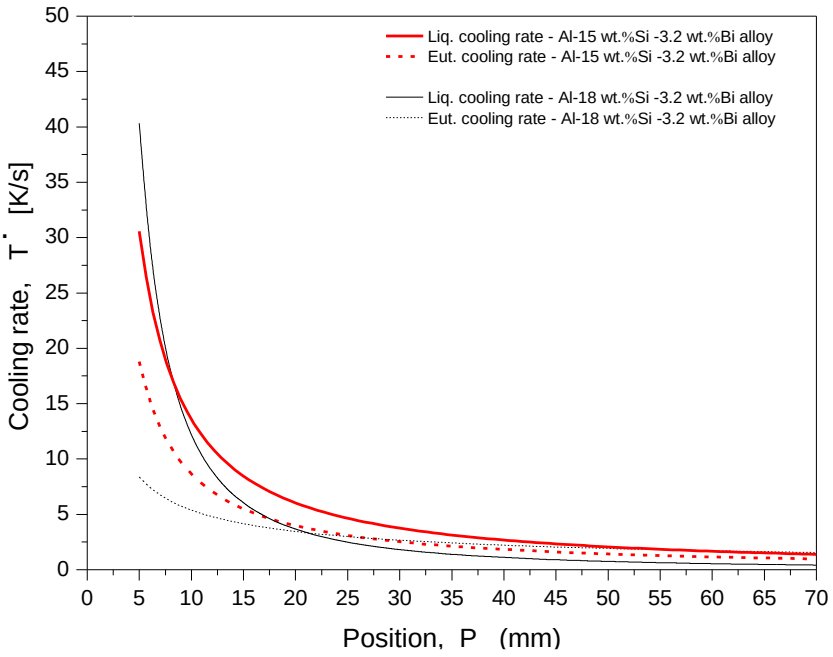

Fig. 5. Cooling rate as a function of position in the Al-Si-Bi alloys castings.

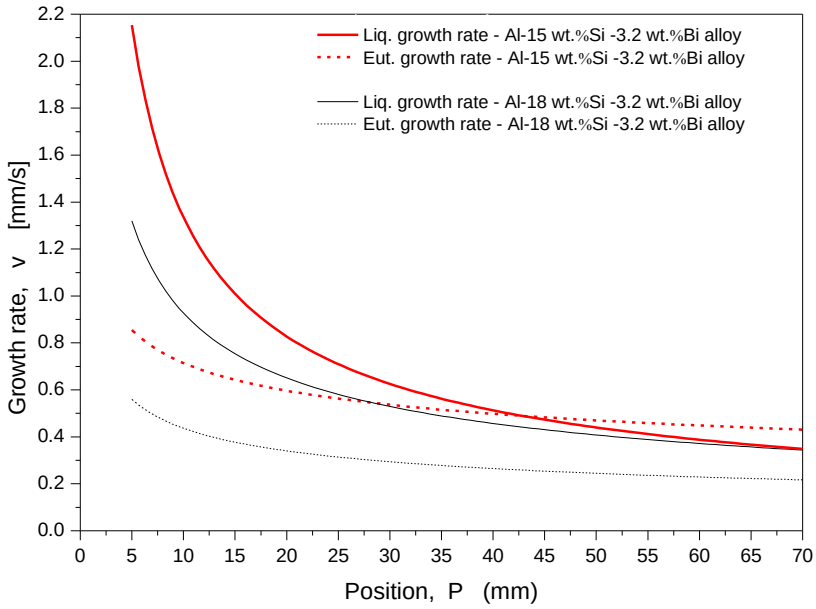

Fig. 6. Growth rate as a function of position in the Al-Si-Bi alloys castings.

Characteristic microstructures of the tested Al-Si-Bi alloys are shown in Fig. 7 and Fig. 8. The lighter areas in each Figure are the α-Al phase, while the dark grey regions are the Si crystals forming both primary and

eutectic structures. The right-side images are the more magnified to show detailing aspects regarding Si morphology. The Bi addition remains in its elemental form within the alloys and it can be seen in light grey areas in the microstructures. From this visualization, the microstructures of the Al-18 wt.%Si- 3.2 wt.%Bi alloy displayed a pro-eutectic Si phase and a (αAl + Si) eutectic structure (Fig. 8). The association of Bi with the experienced cooling rates induced structural modifications in the primary Si phase. As a replacement for the regular polyhedral structures, Bi content modified the primary Si structure to complex crystals with crossing spines. These spines are oriented at approximately 90º with respect to the angular Si. The occurrence of this morphology was also reported by Yilmaz *et al.* [31,32] for an Al-17 wt.%Si alloy containing 0.025 wt.%Sr. The Si morphology of the eutectic structure for the Al-18 wt.%Si- 3.2 wt.%Bi alloy was found to be predominantly flaky lamellar across the casting length.

In the case of the Al-15 wt.%Si- 3.2 wt.%Bi alloy, it is found that the eutectic Si was formed in two distinct morphologies, which are flaky lamellar for slow cooled samples and globular + fibrous for samples solidified at higher rates. The mixture of very fine globules and fibers of eutectic Si is attained for local cooling rates higher than 5 K/s. Likewise reported before for strontium (Sr) [31,32], it appears that Bi enlarge the eutectic Al-Si coupled zone since the growth of primary particles is suppressed for *liquidus* cooling rates higher than 2.0 K/s, (i.e., velocities > 0.4 mm/s). This enlargement can be deduced when compared to the coupled zone in Al-Si alloys for the composition of 15 wt.% Si, as proposed by Atasoy *et al.* [33]. These authors showed that flaky eutectic occurs for higher velocities, around 0.8 mm/s. A less commonly demonstrated morphology of Si crystals can be seen for samples associated with cooling rates below 2.0 K/s. As indicated by arrows in Fig. 7, five-fold branched particles were found. This structure was reported by Kobaiashi and Hogan for slow cooling rates [34].

In both alloys finer microstructures can be seen related to higher cooling rates, which are those related to positions (P) closer to the cooled surface of the casting. The eutectic Si spacing values given in Fig. 7 and Fig. 8 enables comparisons regarding the variation in size of the particles.

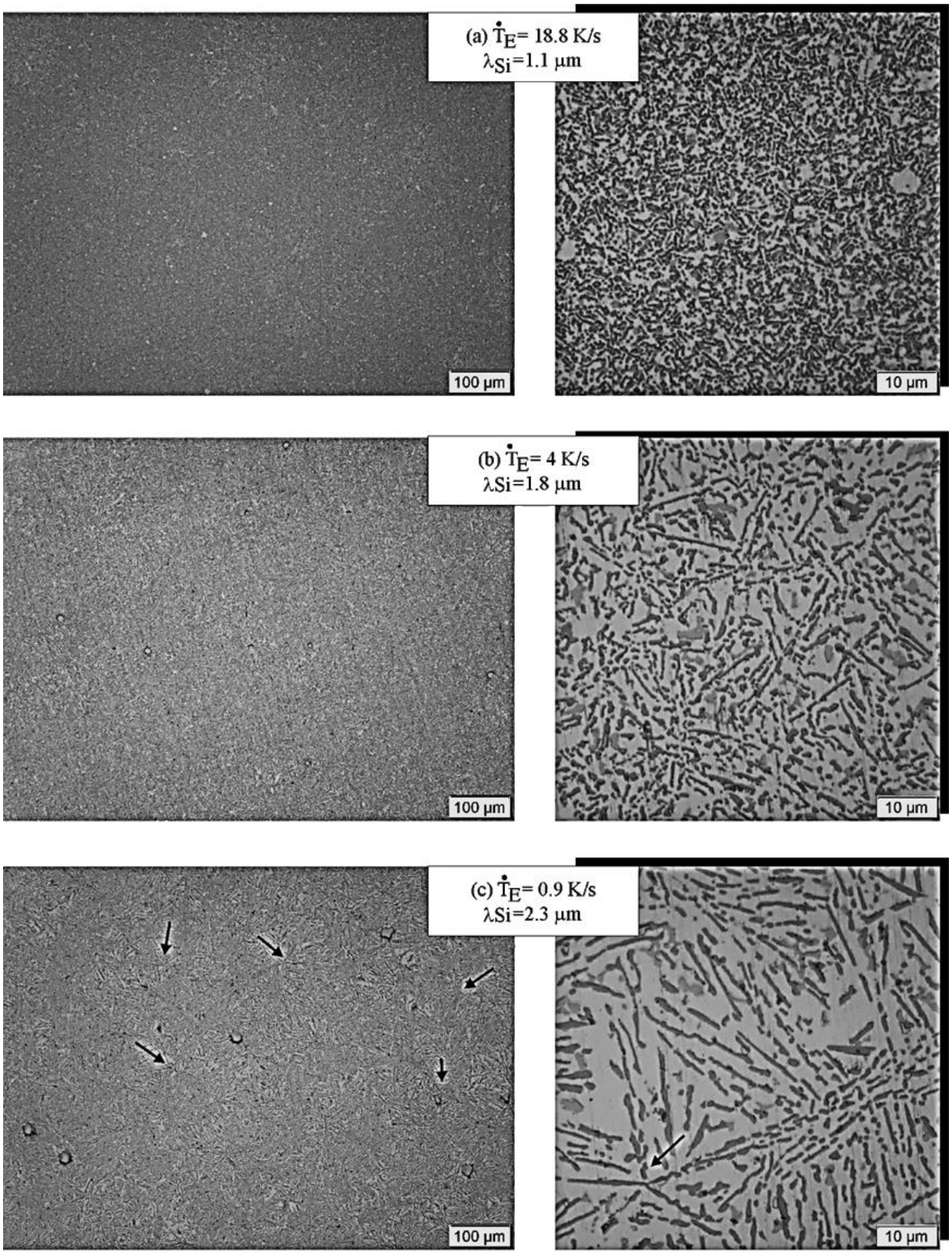

Fig. 7. Typical optical microstructures related to distinct cooling rates of (a) 18.8 K/s, (b) 4 K/s and (c) 0.9 K/s during directional solidification of the Al-15 wt.%Si- 3.2 wt.%Bi alloy casting. Arrows in the images at the bottom indicate the growth of five-fold primary Si for slower cooling conditions.

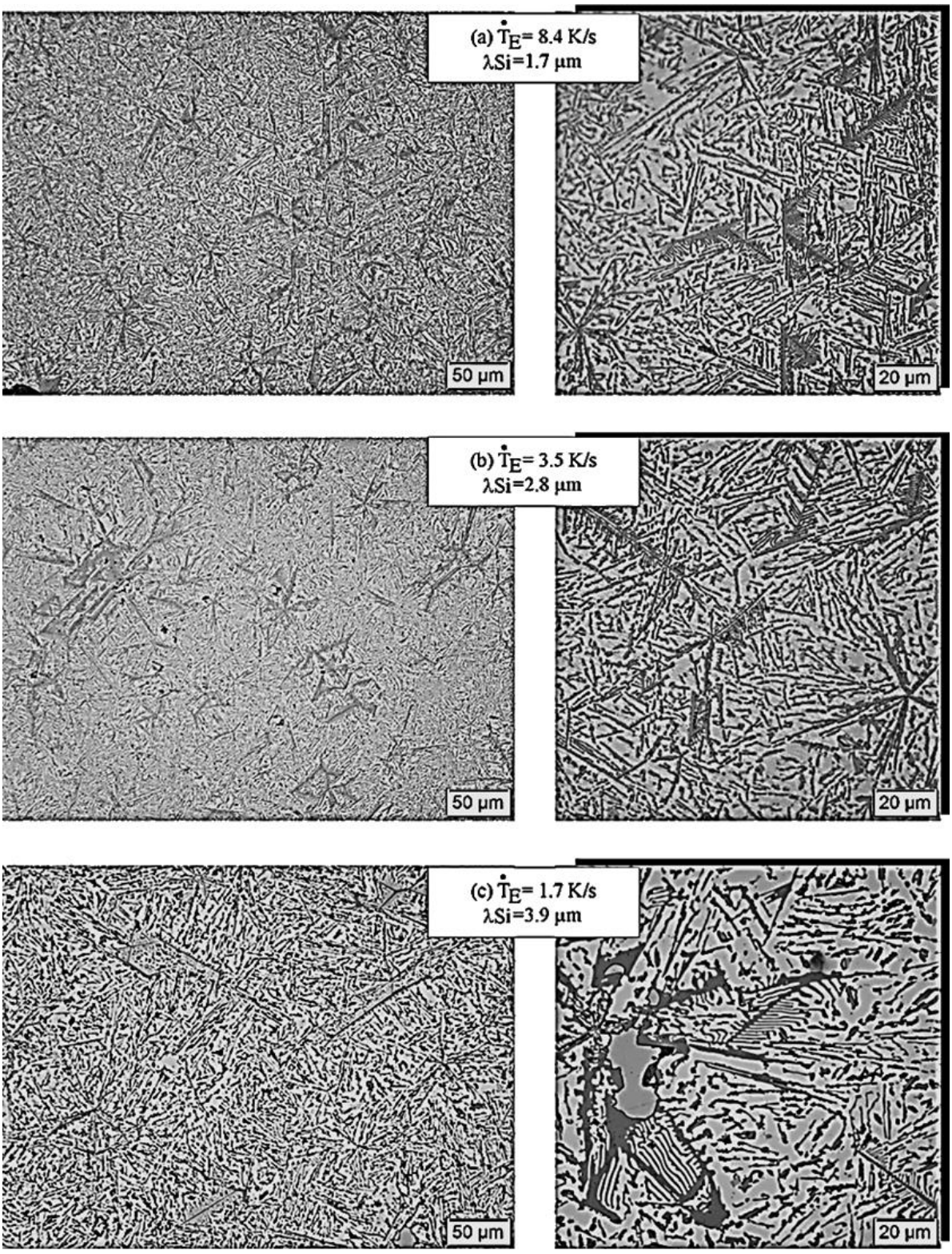

Fig. 8. Typical transverse microstructures related to various cooling rates: (a) 8.4 K/s, (b) 3.5 K/s and (c) 1.7 K/s during directional solidification of the Al-18 wt.%Si- 3.2 wt.%Bi alloy casting.

The presence of the three elements (Al, Bi and Si) can be verified by using elemental SEM-EDS mapping as shown in Fig. 9. As such, the distribution of the elements throughout the microstructure can be also examined. A region of interest containing a primary Si particle was chosen in order to highlight its morphology. The red distinction for Al shows a high intensity associated with the α–Al eutectic phase. The yellow Bi spots can be noted following a quite uniform distribution. Moreover, Si crystals (either eutectic or primary) can be visualized in intense green. The angular Si structure with intersecting spines can be clearly observed.

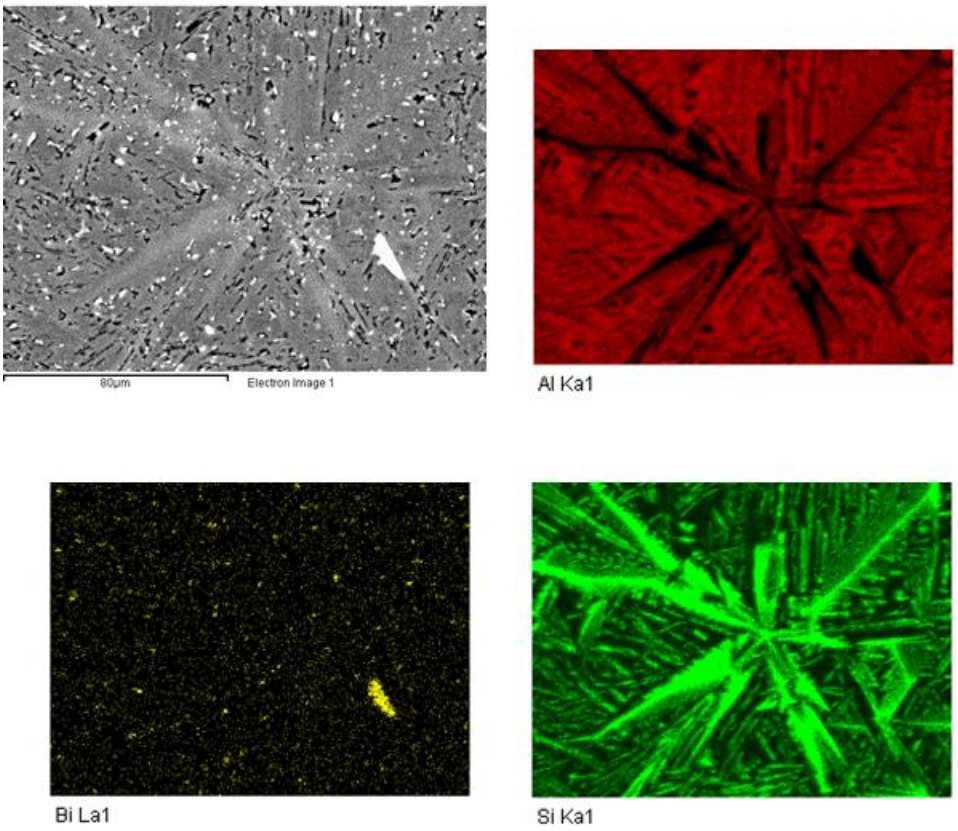

Fig. 9. SEM image in BSE signal of an Al-18 wt.%Si- 3.2 wt.%Bi alloy sample respective X-ray elemental mappings through EDS: Al-K, Bi-L and Si-K.

In order to verify the applicability of the -1/2 growth velocity exponent typical of the Jackson-Hunt (J-H) approach [25, 36-38], the results found for the Al-15 and 18 wt.%Si -3.2 wt.%Bi alloys were compared to previous results of binary Al-15 wt.%Si and Al-18 wt.%Si alloys [35]. This assessment involved a plotting of the eutectic Si spacing versus either the eutectic growth velocity or the eutectic cooling rate, as can be seen in Fig. 10. If one examined Fig 10(a), it is seen that the experimental trend of the Al-15 wt.%Si -3.2 wt.%Bi alloy matches up well the previous function associated with the binary Al-15 wt.%Si alloy, indicating that, in this case, Bi does not affect the Si size. The -1/2 exponent originating from the J-H approach was satisfactorily used to determine

the experimental λ_{Si} x V_E trends for the Al-Si-Bi alloys. With respect to the Al-18 wt.%Si -3.2 wt.%Bi alloy, Bi appears to promote some coarsening on the eutectic Si as compared to the results of the binary Al-18 wt.%Si alloy. The same was observed for microstructural variations with V_E applies to the results for both alloys concerning λ_{Si} x $\dot{T}_E$ as depicted in Fig. 10(b).

Although the individual contribution of the Si alloying on the eutectic Si scale can be said negligible for binary alloys [35], a significant difference can be established in the case of the ternary Al-Si-Bi alloys. As shown in Fig. 10(a), by comparing values of λ_{Si} of both alloys for a given eutectic growth rate, the λ_{Si} of the alloy containing 18 wt.%Si is roughly 70% larger than that found for the Al-15 wt.%Si -3.2 wt.%Bi alloy.

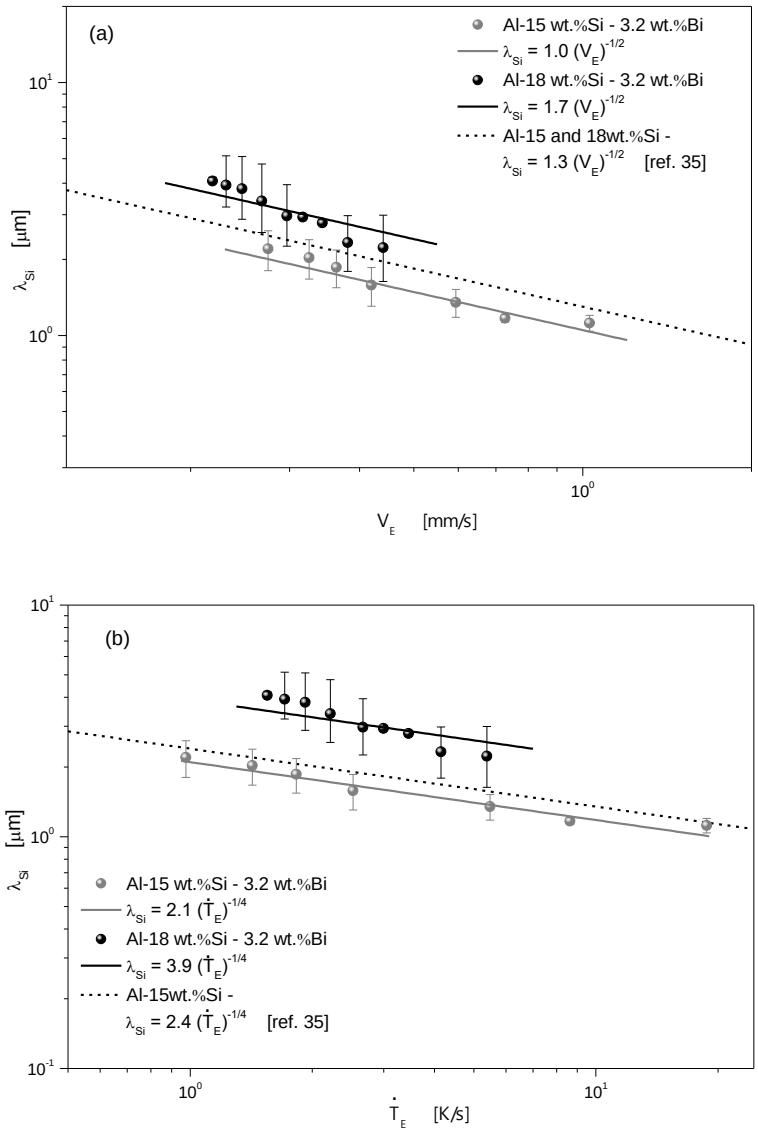

Fig. 10. Variation of the eutectic Si spacing with (a) growth rate and (b) cooling rate plotted for the Al-Si-Bi alloys.

The present results allowed an expression relating the primary Si spacing of the DS Al-18 wt.%Si -3.2 wt.%Bi alloy casting, λ_{Sip}, to the cooling rate to be derived, as can be seen in Fig. 11. Points are experimental results and lines represent an empirical fit to the experimental points. While the eutectic Si spacing was shown to vary with $\dot{T}_E$ according to the relationship $(\lambda_{Si})^4 \times \dot{T}_E$ = constant, the primary Si size (λ_{Sip}) demonstrated to be less sensitive to cooling rate variations, resulting in a relationship $(\lambda_{Sip})^5 \times \dot{T}_L$ = constant.

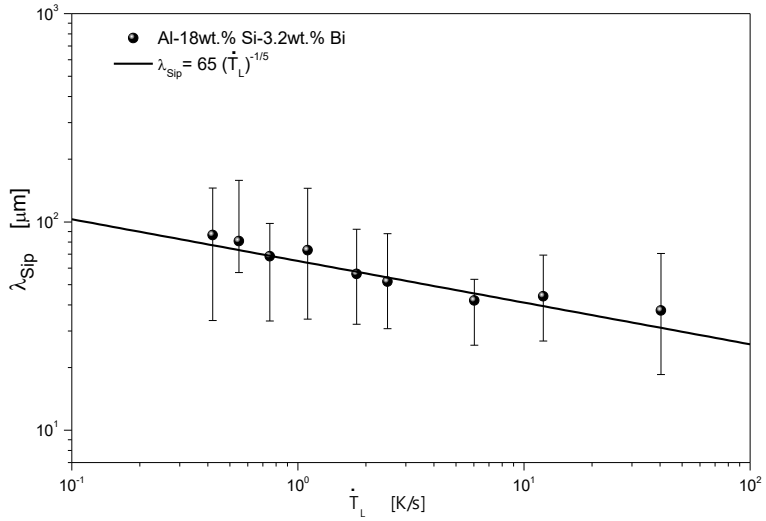

Fig. 11. Variation in primary Si spacing with cooling rate plotted for the DS Al-18 wt.%Si- 3.2 wt.%Bi alloy casting.

As can be seen in Fig. 12, the ultimate tensile strength (σ_u) varies along the length of the DS Al-Si-Bi alloys castings. As previously demonstrated, the quantified aspects of the microstructure are related to the various cooling rates and growth rates determined for the solidified samples. Fig. 12 is proposed to determine if these quantified aspects have an influence in the strength of the Al-15 wt%Si -3.2 wt.%Bi and Al-18 wt%Si -3.2 wt.%Bi alloys. The major microstructural characteristic to be taken in account is the influence of the spacing of the eutectic structure, λ_{Si}. To determine if the scale variation of the spacing influenced the strength and ductility (Fig. 12 and Fig. 13), a method was adopted using a "Hall-Petch" relationship to compare the two tested alloys here as well as the previous results for binary Al-15 wt.%Si and Al-18 wt.%Si alloys [35]. This kind of approach was also demonstrated elsewhere [39,40]. This approach the used method establishes the alloy tensile strength as a function of the microstructural spacing instead of comparing the strength to the grain size.

It can be seen in Fig. 12 that σ_u is more sensitive to $\lambda_{Si}^{-1/2}$ variations along the length of the DS Al-15 wt%Si -3.2 wt.%Bi alloy casting. It appears that the higher proportion of primary Si particles in the Al-18 wt% Si -3.2 wt.%Bi alloy affects the tensile properties, causing lower variation in the tensile properties as can also be observed in Fig. 13 for ductility. The elongation (δ) remains unaltered along the length of the DS Al-18 wt% Si -3.2 wt.%Bi alloy casting, which attests a brittle behavior, since 3% of elongation is roughly obtained. The weak alteration in properties can also be connected to the eutectic Si morphology found to be predominantly flaky lamellar.

On the other hand, σ_u and δ associated with the samples of the Al-15 wt.%Si -3.2 wt.%Bi alloy varied significantly as a function of λ_{Si}. In general, the tensile properties of the alloy containing Al-15 wt.% Si -3.2 wt.%Bi are higher. The behavior of the strength here is in agreement with that reported by Durgrapasadu [23]. This means that the addition of Bi in hypereutectic Al-Si alloys promotes increase in the alloy strength. The positive effect of Bi is very clear if one compares the Hall-Petch plots for ternary and binary compositions in Fig. 12.

The highest σ_u and δ of 205 MPa and 12.5 % for the ternary Al-15 wt.%Si -3.2 wt.%Bi alloy casting are associated with fine microstructural spacings. The average eutectic Si spacing, λ_{Si}, related to those properties is 1.6 μm. In order to achieve the same properties for the same alloy without Bi addition a λ_{Si} of 1.2 μm is required.

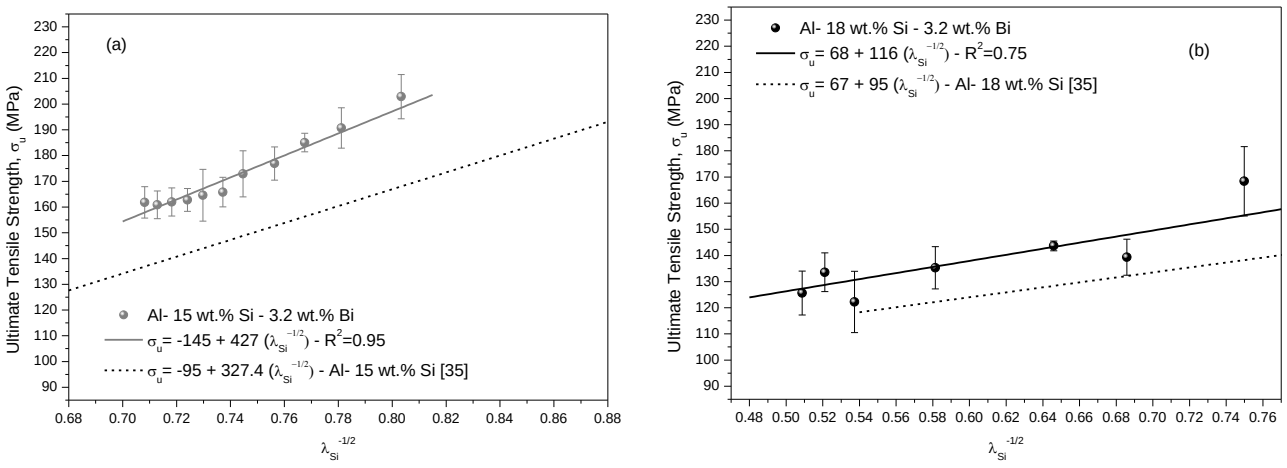

Fig. 12. Evolutions of ultimate tensile strength along the length of the DS (a) Al-15 wt.%Si -3.2 wt.%Bi and (b) Al-18 wt.%Si -3.2 wt.%Bi alloys castings as a function of the Si eutectic spacing. R^2 is the coefficient of determination associated with the adjusted curves.

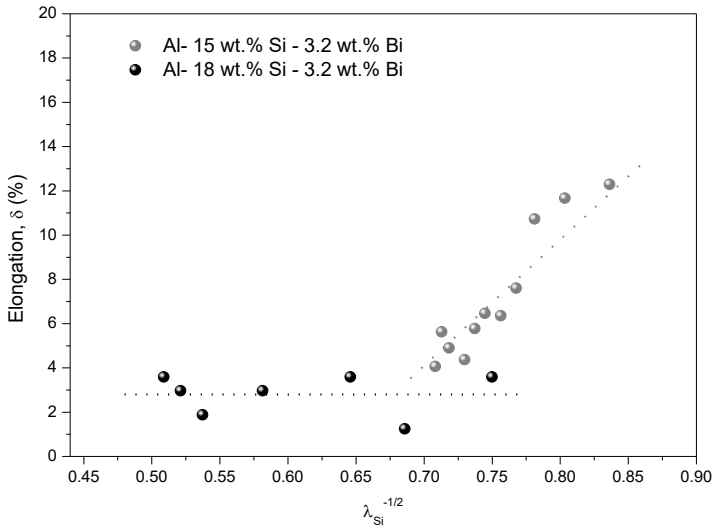

Fig. 13. Elongation along the length of the DS Al-15 wt.%Si -3.2 wt.%Bi and Al-18 wt.%Si -3.2 wt.%Bi alloys castings as a function of the Si eutectic spacing.

4. Conclusions

The following conclusions can be drawn from the present experimental investigation:

- The microstructure of the DS Al-18 wt.%Si- 3.2 wt.%Bi alloy was shown to be characterized by a pro-eutectic Si phase and a (αAl + Si) eutectic mixture. The combined effects of Bi and cooling rate modified the primary Si structure into complex crystals with crossing spines. The Si morphology of the eutectic mixture was found to be predominantly flaky lamellar.
- In the case of the DS Al-15 wt.%Si- 3.2 wt.%Bi alloy casting, it was found that the eutectic Si was formed in two distinct morphologies: flaky lamellar for slowly cooled samples and globular + fibrous for samples solidified at higher cooling rates. A mixture of very fine globules and fibers of eutectic Si occurred for local cooling rates higher than 5 K/s. Five-fold branched Si particles were found to be associated with cooling rates lower than 2 K/s.
- Experimental growth laws are proposed relating the eutectic Si spacing (λ_{Si}) to both the eutectic cooling rate ($\dot{T}_E$) and the growth rate (V_E) for both examined Al-Si-Bi alloys. The -1/2 exponent from the Jackson-Hunt approach was shown to satisfactorily characterize the experimental λ_{Si} x V_E trends. By comparing values of λ_{Si} of both alloys for a given V_E, λ_{Si} of the alloy containing 18 wt.%Si was shown to be about 70% larger than that found for the Al-15 wt.%Si -3.2 wt.%Bi alloy. While λ_{Si} was shown to vary

with $\dot{T}_E$ according to the relationship $(\lambda_{Si})^4 \times \dot{T}_E$ = constant, the primary Si size (λ_{Sip}) demonstrated to be less sensitive to variations in the *liquidus* cooling rate ($\dot{T}_L$), resulting in the following relationship: $(\lambda_{Sip})^5 \times \dot{T}_L$ = constant.

- The addition of Bi in hypereutectic Al-Si alloys was shown to promote increase in the alloy tensile strength. Hall-Petch type experimental relationships were derived relating the ultimate tensile strength (σ_u) to λ_{Si} for both examined Al-Si-Bi alloys. The tensile properties of the Al-15 wt.% Si -3.2 wt.%Bi alloy casting were shown to be higher, attaining highest values of σ_u and elongation (δ) of 205 MPa and 12.5 %, respectively, for a fine λ_{Si} = 1.6 μm. In contrast, a brittle behavior characterized the Al-18 wt.%Si -3.2 wt.%Bi alloy casting, for which δ remained unaltered along the casting length at about 3%.

Data availability

The data that support the findings of this study are available from the corresponding author upon reasonable request.

Conflicts of interest

The author declares no conflicts of interest.

Acknowledgements

The authors are grateful to FAPESP- São Paulo Research Foundation, Brazil (grants 2017/12741-6 and 2018/11791-2), Capes- Coordenação de Aperfeiçoamento de Pessoal de Nível Superior, Brazil (Funding Code 001); and CNPq- National Council for Scientific and Technological Development, Brazil (grant 400506/2016-5).

References

[1] S.O. Tarawanna, A.K. Dahle, 6-Casting of aluminium alloys, in: Fundamentals of aluminium metallurgy: Production, processing and applications, 1th edition, Woodhead Publishing, Edited by: R. Lumley, ISBN: 978-1-84569-654-2 2011; 141-54.

[2] E.L. Rooy, Aluminum Foundry Products, Nonferrous Alloys and Special-Purpose Materials - ASM Metals Handbook 2 1990;1328.

[3] V. Vijeesh, K. Prabhu, Review of Microstructure Evolution in Hypereutectic Al–Si Alloys and its Effect on Wear Properties, Trans. Indian Inst. Met. 2014;67;1-18.

[4] H. Ye, An Overview of the Development of Al-Si-Alloy Based Material for Engine Applications, J. Mater. Eng. Perform. 2003;12; 288-97.
[5] M. Warmuzek, Aluminum-Silicon Casting Alloys: Atlas of Microstructures, ASM International 2016; 186.
[6] B. Korojy, B. Fredriksson, On solidification of hypereutectic Al-Si alloys, Trans. Indian Inst. Met. 2009;62; 361-5.
[7] C.L.Xu, H.Y.Wang, F.Qiu, Y.F.Yang, Q.C.Jiang, Cooling rate and microstructure of rapidly solidified Al-20 wt.% Si alloy, Mater. Sci. Eng. A 2006;417;275–80.
[8] H.S. Kang, W.Y. Yoon, K.H. Kim, M.H. Kim, Y.P. Yoon, Microstructure selections in the undercooled hypereutectic Al–Si alloys, Mater. Sci. Eng. A 2005;404;117-23.
[9] K. F. Kobayashi, L. M. Hogan, The crystal growth of silicon in Al-Si alloys, J. Mater. Sci.1985; 20;1961–75.
[10] T. Hosch, L. G. England and R. E. Napolitano, Analysis of the high growth-rate transition in Al–Si eutectic solidification, J. Mater. Sci. 2009;44;4892–9.
[11] J.E. Spinelli, A.A. Bogno, H. Henein, Two-Zone Microstructures in Al-18Si Alloy Powders, Metall. Mater. Trans. A 2018;49;550-62.
[12] R.V. Reyes, R. Kakitani, T. A. Costa, J.E. Spinelli, N. Cheung, A. Garcia, Cooling thermal parameters, microstructural spacing and mechanical properties in a directionally solidified hypereutectic Al-Si alloy, Phil. Mag. Lett. 2016;96;228-37.
[13] A. Knuutinen, K. Nogita, S.D. McDonald, and A.K. Dahle, Modification of Al-Si Alloys Modified with Ba, Ca, Y and Yb, Light Met. 2001;1;229–40.
[14] G. Timelli, F. Bonollo, Influence of tin and bismuth on machinability of lead free 6000 series aluminium alloys, Mater. Sci. Technol., 2011;27;291-9.
[15] J.F. Kelly, M.G. Cotterell, Minimal lubrication machining of aluminium alloys, J Mater. Process. Technol. 2002;120;327–34.
[16] A. Tomala, M. Rodriguez Ripoll, E. Badisch, Tool – Solid Lubricant – Workpiece Interactions in High Temperatures Applications, Procedia Engineering 2013;68;626–33.
[17] A. Papworth, P. Fox, The disruption of oxide defects within aluminium alloy castings by the addition of bismuth, Mater. Lett. 1998;35;202–6.
[18] M. A. Muftau, United States Patent, Patent Number: 5,122,208, Hypo-eutectic aluminum-silicon alloy having tin and bismuth additions 1992.
[19] Anawati, H. Nordmark, S. Diplas, J. C. Walmsley, K. Nisancioglu, Surface Segregation of Trace Element Bismuth during Heat Treatment of Aluminum. J. Electrochem. Soc. 2012;159;C137-C145.
[20] C.J. Machovec, G.E. Byczynski, J.W. Zindel, L.A. Godlewski, Effect of Bi-Sr Interactions on Si Morphology in a 319-Type Aluminum Alloy, AFS Trans. 2000;108;439–44.
[21] S. Farahany, A. Ourdjini, T. Bakar, M. Idris, On the Refinement Mechanism of Silicon in Al-Si-Cu-Zn Alloy with Addition of Bismuth, Metall. Mater. Trans. A 2014;45;1085–8.

[22] S. Farahany, A. Ourdjini, M.H. Idrsi, S.G. Shabestari, Evaluation of the effect of Bi, Sb, Sr and cooling condition on eutectic phases in an Al–Si–Cu alloy (ADC12) by in situ thermal analysis, Thermochim. Acta 2013;559;59–68.

[23] K. Durgaprasadu, P. Biswas, M. K. Mondal, Study the Effects of Bi Addition on Microstructure and Hardness of Hypereutectic Al17.6Si Alloy, National Conference on Advanced Materials, Manufacturing and Metrology (NCAMMM - 2018) on 16-17, February, 2018 at CSIR-CMERI, Durgapur, 30-34.

[24] M. Okayasu, S. Takeuchi, S. Wu, T. Ochi, Effects of Sb, Sr, and Bi on the material properties of cast Al-Si-Cu alloys produced through heated mold continuous casting, J. Mech. Sci. Technol. 2016;30;1139-47.

[25] K.A. Jackson, J.D. Hunt, Lamellar and rod eutectic growth, Trans. Metall. Soc. AIME 236 (1966)1129-1142.

[26] I. T.L. Moura, C. L.M. Silva, N. Cheung, P. R. Goulart, A. Garcia, J. E. Spinelli, Cellular to dendritic transition during transient solidification of a eutectic Sn 0.7wt%Cu solder alloy, Mater. Chem. Phys. 2012;132; 203-9.

[27] D. M. Rosa, J. E. Spinelli, A. Garcia. Tertiary dendrite arm spacing during downward transient solidification of Al-Cu and Al-Si alloys, Mater. Let. 2006;60;1871-4.

[28] B.Silva, A. Garcia, J.E. Spinelli, Wetting behavior of Sn-Ag-Cu and Sn-Bi-X alloys: insights into factors affecting cooling rate, J. Mater. Res. Technol. 2019;8;1581-6.

[29] N. Cheung, N. S. Santos, J. M.V. Quaresma, G. S. Dulikravich, A. Garcia, Interfacial heat transfer coefficients and solidification of an aluminum alloy in a rotary continuous caster, Int. J. Heat Mass Transfer 2009;52;451-9.

[30] M. Di Sabatino, L. Arnberg, A Review on the Fluidity of Al Based Alloys, Metall Sci Tecnol 2004; 22.

[31] F. Yilmaz, R. Elliott, The microstructure and mechanical properties of unidirectionally solidified Al-Si alloys, J. Mater. Sci. 1989;24;2065–70.

[32] F. Yilmaz, O. A. Atasoy, R. Elliott, Growth structures in aluminium-silicon alloys II. The influence of strontium, J. Crys. Growth 1992;118;377–384.

[33] O.A. Atasoy, F. Yilmaz, R. Elliott, Growth structures in aluminium-silicon alloys I. The coupled zone, J. Crys. Growth, 1984;66;137-146.

[34] K. Kobayashi, L. M. Hogan, Fivefold twinned silicon crystals grown in an A1–16 wt.% Si melt, Phil. Mag. A 1979;40;399-407.

[35] R. V. Reyes, T. S. Bello, R. Kakitani, T. A. Costa, A. Garcia, N. Cheung, J.E. Spinelli, Tensile properties and related microstructural aspects of hypereutectic Al-Si alloys directionally solidified under different melt superheats and transient heat flow conditions, Mater. Sci. Eng. A 2017;685;235-43.

[36] M. Gündüz, J.D. Hunt, The measurement of solid-liquid surface energies in the AlCu, Al-Si and Pb-Sn systems, Acta Metall. 1985;33;1651–72.

[37] M. Gündüz, H. Kaya, E. Çadırli, A. Özmen, Interflake spacings and undercoolings in Al–Si irregular eutectic alloy, Mater. Sci. Eng. A 2004;369;215–29.

[38] P. Magnin, R. Trivedi, Eutectic growth: a modification of the Jackson and Hunt theory, Acta Metall. 1991;39;453–67.

[39] S. Khan, A. Ourdjini, Q.S. Hamed, M.A.A. Najafabadi, R. Elliott, Hardness and mechanical property relationships in directionally solidified aluminium-silicon eutectic alloys with different silicon morphologies, J. Mater. Sci. 1993;28;5957–62.
[40] W. Hearn, J.E. Spinelli, A.A. Bogno, J. Valloton, H. Henein. Microstructure Solidification Maps for Al-10 Wt Pct Si Alloys, Metall. Mater. Trans. A 2019;50;1333-45.

List of figure captions

Fig. 1. Scheme of the upward directional solidification system used to generate the Al-Si-Bi alloy casting: 1 - acquired thermal profiles during experiment; 2 - ceramic support; 3 - electric resistances; 4 - stainless-steel split mold; 5 - thermocouples; 6 - data logger; 7 - water flow inlet; 8 - flowmeter; 9 - temperature controller; 10 - molten alloy and 11 - cooled bottom part.

Fig. 2. Schematic representation of employed methods to measure (a) the primary silicon, λ_{Sip}, and (b) the eutectic Si spacing, λ_{Si}: triangle method for λ_{Sip} and intercept method for λ_{Si}.

Fig. 3. Cooling curves at different positions within the DS (a) Al-15 wt.%Si-3.2 wt.%Bi and (b) Al-18 wt.%Si-3.2 wt.%Bi alloys castings. The signs within the graphs signify the positions in mm from the cooled surface of the casting.

Fig. 4. Pseudo-binary Al-3.2 wt%Bi – (X)Si phase diagram computed using TCAL3 database of the Thermo-Calc software with signs of the studied chemistries.

Fig. 5. Cooling rate as a function of position in the Al-Si-Bi alloys castings.

Fig. 6. Growth rate as a function of position in the Al-Si-Bi alloys castings.

Fig. 7. Typical optical microstructures related to distinct cooling rates of (a) 18.8 K/s, (b) 4 K/s and (c) 0.9 K/s during directional solidification of the Al-15 wt.%Si- 3.2 wt.%Bi alloy casting. Arrows in the images at the bottom indicate the growth of five-fold primary Si for slower cooling conditions.

Fig. 8. Typical transverse microstructures related to various cooling rates: (a) 8.4 K/s, (b) 3.5 K/s and (c) 1.7 K/s during directional solidification of the Al-18 wt.%Si- 3.2 wt.%Bi alloy casting.

Fig. 9. SEM image in BSE signal of an Al-18 wt.%Si- 3.2 wt.%Bi alloy sample respective X-ray elemental mappings through EDS: Al-K, Bi-L and Si-K.

Fig. 10. Variation of the eutectic Si spacing with (a) growth rate and (b) cooling rate plotted for the Al-Si-Bi alloys.

Fig. 11. Variation in primary Si spacing with cooling rate plotted for the DS Al-18 wt.%Si- 3.2 wt.%Bi alloy casting.

Fig. 12. Evolutions of ultimate tensile strength along the length of the DS (a) Al-15 wt%Si -3.2 wt.%Bi and (b) Al-18 wt%Si -3.2 wt.%Bi alloys castings as a function of the Si eutectic spacing. R^2 is the coefficient of determination associated with the adjusted curves.

Fig. 13. Elongation along the length of the DS Al-15 wt%Si -3.2 wt.%Bi and Al-18 wt%Si -3.2 wt.%Bi alloys castings as a function of the Si eutectic spacing.